



ELSEVIER

Surface Science 395 (1998) 342–355

surface science

Lateral forces and atomic desorption induced by the electric field created by STM tips on metal surfaces

N. Mingo *, F. Flores

Departamento de Física Teórica de la Materia Condensada C-V, Facultad de Ciencias, Universidad Autónoma de Madrid, Madrid 28049, Spain

Received 7 March 1997; accepted for publication 21 July 1997

Abstract

The effect of the electric field created by an external voltage at a scanning tunneling microscope interface is analyzed by means of a self-consistent LCAO approach. The theoretical method introduced in this paper allows us to analyze realistic tip-sample geometries without introducing spurious two-dimensional periodicities. We present results for both the lateral forces acting on different alkali atoms adsorbed on an Al(100) sample and the atomic desorption potential induced by an external voltage. The evaporation fields for Na and K are calculated for different tip-sample distances, and the results are in good agreement with the experimental evidence. © 1998 Elsevier Science B.V.

Keywords: Ab initio quantum chemical methods and calculations; Alkali metals; Aluminium; Green's function methods; Scanning tunneling microscopy; Surface diffusion

1. Introduction

Electric-field induced ionization has been used since the invention of the field ion microscope [1]. With the advent of STM [2], different groups [3,4] have been able to control the position of atoms on metal or semiconductor surfaces by applying an appropriate voltage between the microscope tip and the sample. Moreover, by adjusting the sign and the magnitude of the voltage, atoms have also been transferred between the tip and the sample [3,5]. Accordingly, one of the main theoretical issues in the STM field is to understand and quantify both the lateral forces acting on the adsorbed atoms at the interface and the atomic

desorption potential induced by an external voltage.

Using a density functional (DF) approach, Kreuzer et al. [6] and Neugebauer and Scheffler [7] have studied the effect of a uniform electric field on the desorption of atoms chemisorbed on metal surfaces, while Buldum and Ciraci [8] have analyzed the lateral forces and the atomic switch induced between two metal slabs. More realistic geometries simulating the tip-sample configuration have been introduced by Hirose and Tsukada [9] within a DF approach, although they used a (2×2) parallel periodicity which might mesh some of the effects associated with the atomic desorption due to the ion-ion interaction between different cells of the (2×2) supercell.

Linear combination of atomic orbitals (LCAO) methods [10,11] have also been used to study the

* Corresponding author. Fax: (+34) 1 3974950
e-mail: natalio@uamca0.fmc.uam.es

desorption of atoms and molecules from small clusters in the presence of very high fields. While these calculations have given useful results for understanding electric-field induced ionization processes in the field ion microscope, the geometries considered are far from the realistic geometries appearing in the scanning tunneling microscope.

Realistic tip-sample geometries free of the problems introduced by a fictitious parallel periodicity or by small clusters have only been considered in the analysis of the van der Waals forces [12,13] arising in the microscope.

The aim of this paper is to consider realistic STM geometries [13] and analyze the effect of the electric fields induced between the tip and the sample on the chemisorption energy of atoms (Na and K) adsorbed on metal surfaces (Al(100)). In our approach, we use an LCAO method [14,15], which is presented in Section 2 along with our model. Section 3 is devoted to discussing the Green's function techniques [16] used to solve the realistic geometry analyzed in this paper. We should comment that in the solution presented here, we have neglected the tunneling currents induced between the tip and the sample [9]. This is a reasonable approximation for the tip-sample distances analyzed in this paper (between 15 and 19 a.u.), a regime for which the microscope conductance is at least 3 or 4 orders of magnitude smaller than the quantum unit $2e^2/h$, a value which can be expected to appear for a tip-sample close contact [17]. In Ref. [18], we discussed how to calculate these tunneling currents by means of the LCAO approach used in this paper. We shall assume throughout this work, however, that the tunneling currents modify only very slightly the calculated solution, taking them as equal to zero. In Section 4 our main results will be presented, and Section 5 will be devoted to conclusions and final remarks.

2. Model and general method of solution

Fig. 1 shows the general geometry of the STM interface we are going to analyze, with an alkali atom adsorbed on an Al(100) surface. The metal tip is also assumed to be Al, although we consider

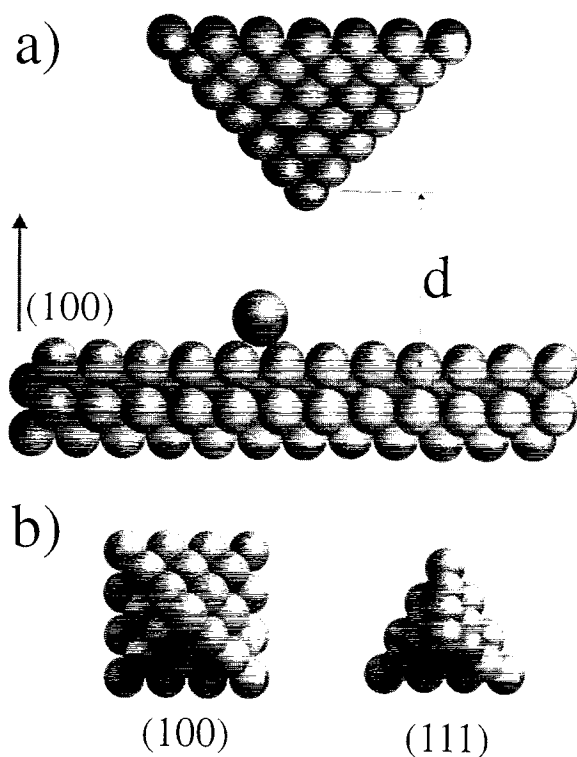


Fig. 1. (a) STM interface geometry. (b) Different tip geometries considered in this paper.

two different tip orientations (Fig. 1b) along the (100) and the (111) directions. The tip geometry has seven layers, and this cluster is assumed to be joined to a reservoir fixing its chemical potential. Notice that the Al tips have not been prepared to comply with this model, although one could expect these tips to exist after making contact between the initial tip and the Al sample. Anyway, as discussed below, in our analysis we shall mainly concentrate our interest on analyzing the chemical properties of the K–Al(100) bond, in such a way that the main role played by the tip will be to create the electric field acting on the alkali atom–metal interface.

The chemical properties of the K(Na)–Al bond will be analyzed using an LCAO-LD (linear combination of atomic orbitals local density) method which has been introduced elsewhere [14,15,19]. The method has been applied successfully to the calculation of the properties of different alkali atoms chemisorbed on metals or semiconductors.

In the rest of this section, we present a summary of its main features; for more details the reader is referred to Refs. [14,15].

In our LCAO approach, we introduce an atomic basis formed by the sp^3 valence orbitals of Al (3s and 3p orbitals) and the s-valence orbital of Na 3s or K 4s. In this basis, the electronic properties of the system are described by the following Hamiltonian:

$$H = H^{oc} + H^{mb}, \quad (1)$$

where

$$H^{oc} = \sum_{i,\sigma} E_i n_{i\sigma} + \sum_{i,j,\sigma} T_{ij} C_{i\sigma}^+ C_{j\sigma} \quad (2)$$

defines the one-electron part of Eq. (1), and

$$H^{mb} = \sum_i U_i n_{i\uparrow} n_{i\downarrow} + \frac{1}{2} \sum_{i \neq j, \sigma} [J_{ij}^{(o)} n_{i\sigma} n_{j\sigma} + \tilde{J}_{ij}^{(o)} n_{i\sigma} n_{j\sigma}] \quad (3)$$

defines its many-body contribution. The different levels E_i of each orbital i and the hopping integrals T_{ij} are obtained using tabulated [20] atomic wave functions for the valence orbitals mentioned above, and the theoretical expressions given in Refs. [14,15].

In Eq. (3), $U_i^{(o)}$, $J_{ij}^{(o)}$ and $\tilde{J}_{ij}^{(o)}$ define the intrasite and intersite Coulomb interactions associated with the atomic wavefunctions Ψ_i and Ψ_j . In Refs. [14,15], we have discussed how the many-body Hamiltonian (Eq. (3)) can be reduced to an effective Hamiltonian using a Kohn–Sham approach. In this scheme, we introduce the following Hartree and exchange correlation potentials:

$$V_{i\sigma}^H = \frac{\partial E^H[n_{i\sigma}]}{\partial n_{i\sigma}}, \quad V_{i\sigma}^{XC} = \frac{\partial E^{XC}[n_{i\sigma}]}{\partial n_{i\sigma}}, \quad (4)$$

E^H and E^{XC} being the Hartree and exchange correlation energies, written as a function of the orbital occupation numbers $n_{i\sigma}$. Then, Eq. (1) is replaced by the following Kohn–Sham effective Hamiltonian:

$$H^{eff} = H^{oc} + \sum_{i\sigma} [V_{i\sigma}^H + V_{i\sigma}^{XC}] n_{i\sigma}. \quad (5)$$

The Hartree energy is given by

$$E^H[n_i] = \sum_i U_i n_{i\uparrow} n_{i\downarrow} + \frac{1}{2} \sum_{i \neq j, \sigma} [J_{ij}^{(o)} n_{i\sigma} n_{j\sigma} + \tilde{J}_{ij}^{(o)} n_{i\sigma} n_{j\sigma}], \quad (6)$$

while the exchange-correlation term takes the approximate form

$$E^{XC}[n_i] = -\frac{1}{2} \sum_{i\sigma} J_i n_{i\sigma} (1 - n_{i\sigma}) - \frac{1}{2} \sum_{i\sigma} f_i (U_i - J_i) n_{i\sigma} (1 - n_{i\sigma}), \quad (7)$$

the exchange term $-\frac{1}{2} \sum_{i\sigma} J_i n_{i\sigma} (1 - n_{i\sigma})$ is given by the interaction between the charge $n_{i\sigma}$ and its exchange hole $1 - n_{i\sigma}$. The correlation term also represents the interaction of the charge and its correlation hole $f_i(1 - n_i)$ (details about the factor f_i can be found in Refs. [14,15]).

The chemical bond between the alkali atom and the metal surface is analyzed by solving Eq. (5). We should comment that in our calculations (for the alkali atom closer to the sample than to the tip) we neglect, as mentioned in Section 1, the hopping integrals T_{ij} between the adatom and the tip. Obviously, we cannot neglect the electrostatic potential the tip induces on the sample or the adatom, since that potential plays a fundamental role in the problem in which we are interested.

Eq. (5) has to be solved self-consistently, since the occupation numbers n_i defining the many-body potential $V_i^H + V_i^{XC}$ depend on this same local potential. In our general approach we use Green's function techniques [16] and project the semi-infinite metal surface onto the last four layers. This procedure allows us to reduce the total problem to a metal film of four layers, the adsorbed species (either K or Na), and the tip. This problem is still very complicated, and it is usually reduced to a simpler one by introducing some periodicity parallel to the surface. In the Section 3, we present the method we have used to treat the geometry of a single tip without resorting to spurious periodicities.

3. Effective electrostatic matrix

In our self-consistent procedure, one starts with a given initial Hamiltonian (Eq. (5)) and calculates n_i . In the next step, a new many-body potential $V_i^H + V_i^{XC}$ is obtained using the new occupation numbers n_i , and the cycle is repeated until a given self-consistency in the charges n_i and potentials $V_i^H + V_i^{XC}$ is obtained.

In our method of analyzing the geometry shown in Fig. 1, we proceed as follows. First, we divide our system into two parts, A and B (see Fig. 2). Region A represents the area on the metal surface where we assume the adatom and the tip to introduce the strongest perturbation. Region B is assumed to be only slightly perturbed. Then, we assume that in region B, the perturbation potential V_i^B induces the following charge n_i^B :

$$n_i^B = \sum_j \chi_{ij}^{BB} V_j^B, \tag{8}$$

where the sum extends to all sites and orbitals belonging only to region B.

Crucial assumptions in Eq. (8) are the linearity between n_i^B and V_j^B , and that the charge n_i^B only depends on the potential induced in the same

region B. This is a plausible approximation, because at long distances from the tip–adatom region, the induced potential should change very slowly with distance, and a linear Fermi–Thomas approximation will be valid with n_i^B proportional to V_i^B . Metal surfaces can be expected to be always within the limits of applicability of this approximation. However, semiconductors, where the screening length is very large, cannot be analyzed in this way. The electronic polarizability X_{ij}^{BB} of the metal is determined, in linear theory, by using the Green’s function $G_{ij}^{(0)}(\omega)$, defined by

$$G_{ij}^{(0)} = (\omega \delta_{ij} - H_{ij}^{(0)})^{-1} \tag{9}$$

where $H_{ij}^{(0)}$ is the unperturbed Hamiltonian of the Al metal surface. $G_{ij}^{(0)}(\omega)$ is calculated using the decimation technique presented in Ref. [16], and then χ_{ij}^{BB} is given by

$$\chi_{ij}^{BB} = \frac{1}{2\pi} \text{Im} \int_{-\infty}^{E_F} G_{ij}^{(0)}(\omega) G_{ij}^{(0)}(\omega) d\omega. \tag{10}$$

In our calculations, only the diagonal term $i=j$ contributes substantially to the induced charge n_i^B , as corresponds to a Fermi–Thomas approximation.

In general, in Eq. (8) V_j^B refers to the total potential acting on the orbital j . We have found that for the purposes of this work, this equation can be well approximated by neglecting the exchange and correlation contributions. The main reason for this result is the long-range character of the electrostatic potential induced at the interface: the short-range, many-body terms only introduce slight changes in the induced charge at each site. Thus, in our approach we have substituted Eq. (8) for

$$n_i^B + \sum_j \chi_{ij}^{BB} V_{H,j}^B, \tag{11}$$

where $V_{H,j}^B$ is only the Hartree potential.

We are going to use Eq. (11) to reduce the total self-consistent problem in the region A+B to an effective self-consistent problem in the reduced area A.

To this end, consider the self-consistent Hartree potentials V_H^A and V_H^B and their relation to the

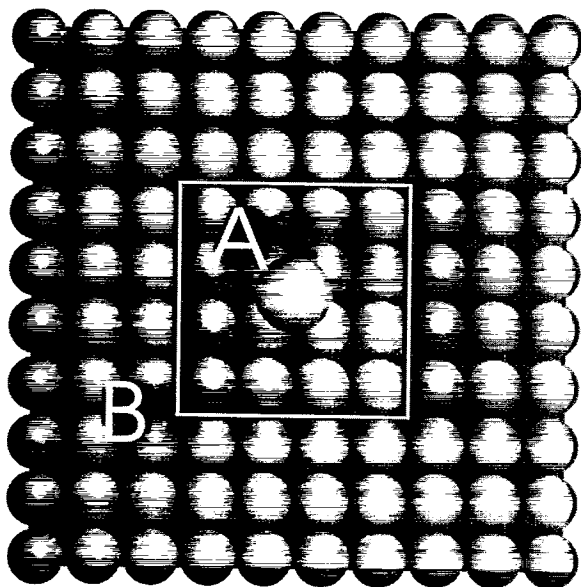


Fig. 2. The interface is divided into regions A and B. Region A is localized around the adsorbed atom.

induced charges n^A and n^B

$$V_{\text{H}i}^A + \sum_j v_{ij}^{AA} n_j^A + \sum_j v_{ij}^{AB} n_j^B, \quad (12)$$

$$V_{\text{H}i}^B = \sum_j v_{ij}^{BA} n_j^A + \sum_j v_{ij}^{BB} n_j^B, \quad (13)$$

where v^{AA} , v^{AB} and v^{BB} define the Coulomb potentials created by the different charges. It is convenient to rewrite Eqs. (11)–(13) in matricial form

$$n^B = \chi^{BB} V^B, \quad (14)$$

$$V_{\text{H}}^A = v^{AA} n^A + v^{AB} n^B, \quad (15)$$

$$V_{\text{H}B} = v^{BA} n^A + v^{BB} n^B. \quad (16)$$

Then, eliminating n^B and V^B from Eqs. (14)–(16), we obtain

$$V_{\text{H}A} = [v^{AA} + v^{AB} \chi^{BB} (I - v^{BB} \chi^{BB})^{-1} v^{BA}] n^A. \quad (17)$$

This is the basic equation allowing us to include the effect of region B in the self-consistent equations for region A. In this method we replace the effect of region B by the effective potential v_{eff}^{AA} linking V_{H}^A and n^A . Thus, instead of v^{AA} , we have to use the effective Coulomb interaction

$$v_{\text{eff}}^{AA} = v^{AA} + v^{AB} \chi^{BB} (I - v^{BB} \chi^{BB})^{-1} v^{BA}. \quad (18)$$

Then, we solve the sample–adatom–tip problem in the reduced region A, and introduce the effect of region B through the effective Hartree potential defined by Eqs. (17) and (18). Notice that the main difficulty of this method is to obtain $(I - v^{BB} \chi^{BB})^{-1}$; this is calculated only once, and is used later on in each step of the self-consistent procedure. In practice, we can easily introduce in our calculations a region B extending up to 10–14 cells away from the adsorbed atom, and reduce the full non-perturbative self-consistent calculation to a restricted area A, having a size of only 3×3 .

It should also be noted that the electronic structure of the reduced area A is obtained using the Green's function techniques already presented in Ref. [16], and determining, in a first step, the different components $G_{ij}^{(0)}(\omega)$ ($i, j \in A$) of the ideal metal surface. In this approach, we neglect the small perturbation which the Hartree potential V_{H}^B introduces into the Green's function $G_{ij}^{(0)}$ of region A. In a further step, this Green's function is perturbed by the different interactions between

the metal and the adsorbed atom or the tip. The crucial point to realize is that the combination of this Green's function technique and of the effective Coulomb interaction discussed above reduces the general problem to calculating self-consistently V_i and n_i around the reduced region A.

4. Results

First, we have analyzed the electrostatic interaction between an Al tip and a clean Al(100) surface. For this case, we have only calculated self-consistently the electric field at the tip–sample surface, and have neglected any other effects like surface relaxation, etc. This means that for the tip and the sample, we have used the tight-binding parameters taken from Ref. [21], and have only obtained the electronic charge induced on both surfaces, introducing the self-consistent equations between that induced charge n_i and the energy levels E_i of each orbital. In this self-consistency, Eqs. (17) and (18) have been used to reduce the total self-consistent equations to a small area around the center of the tip.

Figs. 3a and b show our results for the (100) and (111) Al tips for a tip–sample distance of 19 a.u. and a bias of 9 V, with the apex atom of the tip located above a surface hollow site. Notice the similarities between the two cases, even though the Al(111) tip is sharper and creates an electric field which changes more rapidly in the direction perpendicular to the surface. This tip creates a maximum electric field of 0.34 V \AA^{-1} on the metal surface, while for the (100)-oriented tip this field is 0.42 V \AA^{-1} . These values should be compared with the mean electric field (0.90 V \AA^{-1}) associated with the bias (9 V) and the distance (19 a.u.). Obviously, the effect of the tip geometry is to increase the mean electric field near the tip and to reduce it by more than a factor of 2 at the metal surface. We have explored the linearity of the induced field with respect to the applied voltage, and have found that, for the geometries analyzed in this paper, when there is no alkali atom adsorbed on the surface, the system behaves with a high linearity at least for $-9 \text{ V} < V < 9 \text{ V}$. This result is easily understood

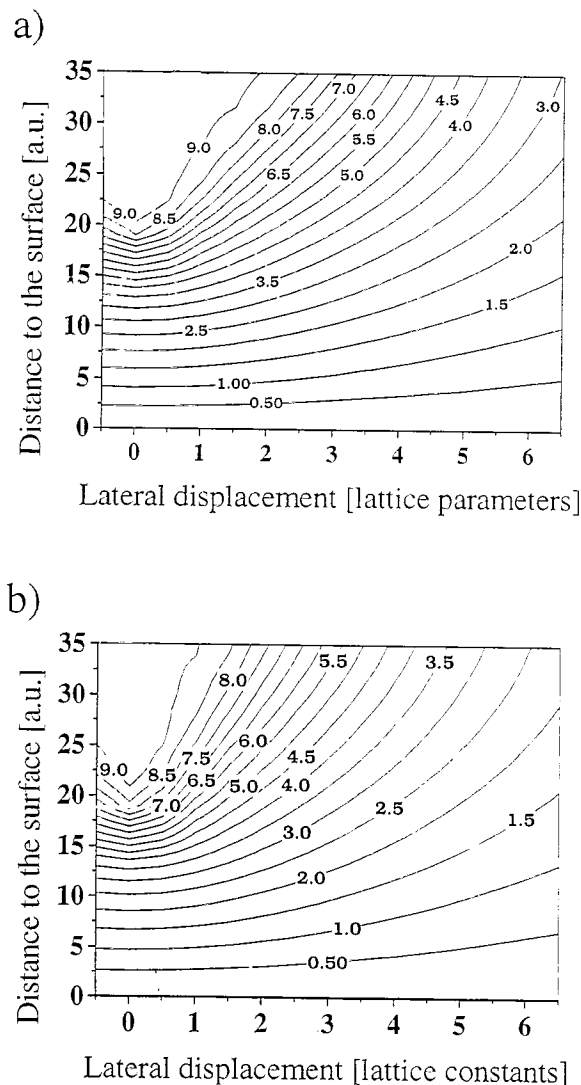


Fig. 3. Electrostatic potential at the STM interface for $d=19$ a.u. and $V=9$ V. (a) (100) tip orientation, (b) (111) tip orientation.

by realizing that the maximum electronic charge induced on the Al atoms is always small compared with its total valence charge of three electrons. We have found that this linearity also applies to a tip-sample distance of 15 a.u. For these smaller distances, the electric field resembles very much the results of Fig. 3, and its values can be obtained from Fig. 3 by a simple scaling with the distance. As the differences between the electric fields created by the (111)- and (100)-oriented tips on the metal

are rather small, in the following discussion we will present our results for the adsorbed alkali atom considering only the (100)-oriented tip.

We now turn our attention to the case of a tip-alkali atom-sample configuration with the apex atom of the tip located above a hollow site of the Al(100) surface. We have applied the general method explained in Section 2 to the calculation of the chemisorption energy of a Na (or K) atom located at the interface. Fig. 4 shows the chemisorption energy for Na as a function of its coordinates in the z - x plane (z is perpendicular to the surface and x goes along the (010) direction) for $d=19$ a.u. and $V=-9, -3, 3$ and 9 V. The different curves in Fig. 4 correspond to constant chemisorption energies. Notice the evolution of the chemisorption energies and the different barrier heights as a function of the applied bias. For $V=\pm 3$ V, the structure of the chemisorption wells is not changed greatly by the applied voltage. The maximum chemisorption energy just below the tip center is 1.64 and 1.27 eV for $V=+3$ and -3 V, respectively. These values should be compared with 1.43 eV, the chemisorption energy for $V=0$. The main effect of a positive (negative) voltage is to create an electric field near the surface which attracts (repels) the ion towards (from) the tip. Fig. 5 shows the adatom chemisorption energy along the dotted lines shown in Fig. 4: these curves measure the importance of the attractive or repulsive well induced by the tip bias. Figs. 4 and 5 also show similar results for $V=\pm 9$ V. For these cases, the effects already appearing for $V=\pm 3$ V are much more pronounced. In particular, for 9 V we see that the barrier heights for the motion of the atom parallel to the surface have been reduced to around 0.01 eV. We have also found that the atomic potential well along the metal surface, induced by the tip-sample voltage, can be described well by the following function:

$$\frac{\delta E_0}{[1 + (\rho/\rho_0)^2]^3} \quad (19)$$

where δE_0 is the maximum well depth, ρ_0 is a length measuring the well width, and ρ is the distance to the center of the well. Table 1 gives

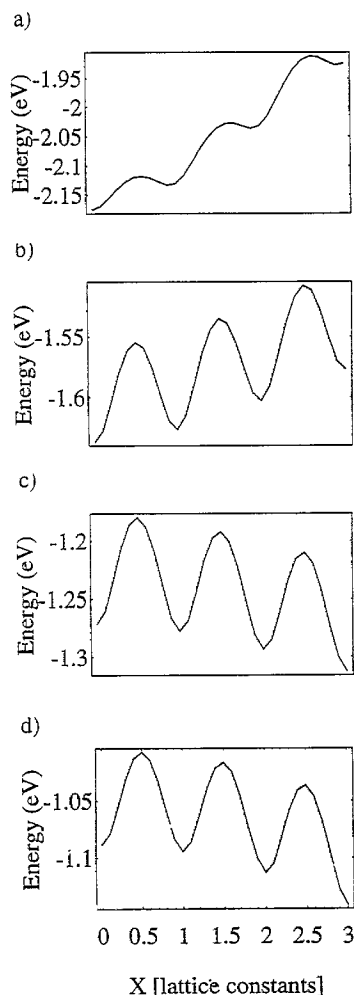
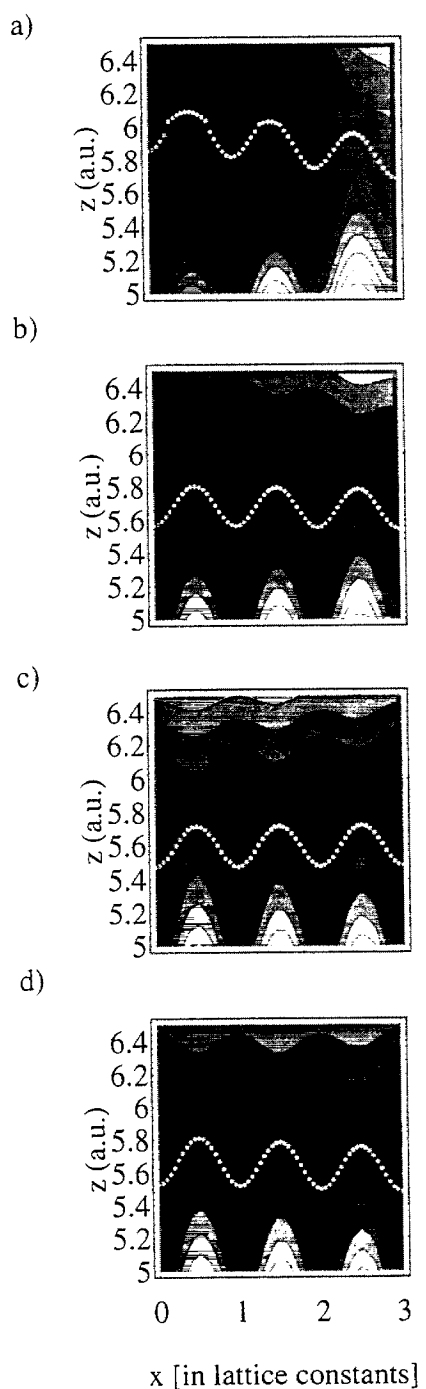


Fig. 5. Na chemisorption energy along the dotted lines of Fig. 6. (a) $V=9$ V, (b) $V=3$ V, (c) $V=-3$ V, (d) $V=-9$ V.

different values of δE_0 and ρ_0 as a function of d and the applied bias V .

Regarding the motion of the atom in the direction perpendicular to the surface, in Fig. 6 we have drawn the chemisorption energy of Na as a function of the atom–metal distance for different

Fig. 4. Curves of constant chemisorption energy for Na adsorbed on Al(100), $d=19$ a.u., and (a) $V=9$ V, (b) $V=3$ V, (c) $V=-3$ V, (d) $V=-9$ V. The straight line ($x=0, z$) is perpendicular to the surface and goes from a surface hollow site to the center of the tip-apex atom. The scale of energies can be taken from Figs. 5 and 6. Contours are taken every 0.05 eV.

Table I
 δE_0 and ρ_0 define the potential well induced parallel to the surface (Eq. (19)) for different values of V and d

	V	δE	ρ_0
(a) Na, $d=19$ a.u.	+9.0	-0.34	8.92
	+3.0	-0.16	6.12
	-3.0	+0.21	5.88
	-9.0	+0.73	5.12
(b) Na, $d=15$ a.u.	+6.0	-0.34	6.23
	+2.0	-0.5	4.80
	-2.0	+0.19	4.47
	-6.0	+0.69	3.95
(c) K, $d=19$ a.u.	+5.0	-0.22	9.36
	+2.5	+0.20	6.23
	-2.5	+0.49	5.09
	-5.0	+0.49	4.42
(d) K, $d=17$ a.u.	+3.5	-0.20	7.12
	+2.0	-0.14	5.98
	-2.0	+0.20	5.16
	-3.5	+0.39	3.57

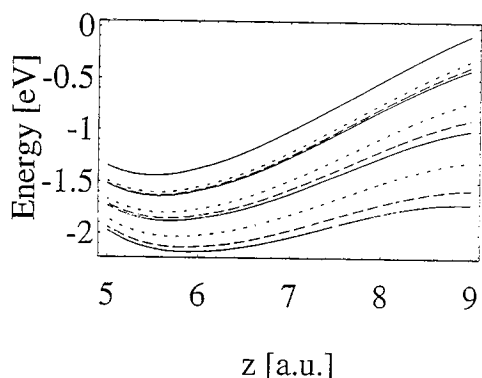


Fig. 6. Na chemisorption energy for $d=19$ a.u. along different straight lines perpendicular to the surface. Full lines: ($x=0, z$) and $V=0, 3, 6$ and 9 V. Short-dashed lines: ($x=1$ lattice constant, z) and $V=3, 6$ and 9 V. Long-dashed lines: ($x=2$ lattice constants, z) and $V=3, 6$ and 9 V.

applied positive voltages and $d=17$ a.u. This energy is shown for different straight lines perpendicular to the surface, passing by the tip center (solid line) and displaced by 1 and 2 lattice distances (long- and short-dashed lines, respectively; 1 lattice distance = 5.4 a.u.). From Fig. 6 we can obtain the behavior of the barrier height for the transfer of Na from the sample to the tip as a function of the applied voltage. Thus, we see that the initial barrier of 1.43 eV is reduced to 0.3 and 0.0 eV for $V=9$ V and $V=12$ V, respectively. It is

obvious that for $V=10$ V and room temperature, we can expect the atom to be transferred from the sample to the tip.

Figs. 7–9 show our results for Na and $d=15$ a.u. In Fig. 7 we present constant chemisorption energy curves in the $x-z$ plane. Fig. 8 shows the chemisorption energy along directions parallel to the surface, and Fig. 9 shows the same energy for several perpendicular directions. Figs. 10–12 present similar results for K and $d=19$ a.u., while Figs. 13–15 show the case of K for $d=17$ a.u.

From these curves we see that for Na, the atomic transfer is achieved for a substantially smaller applied bias if the tip-sample distance is reduced from 19 to 15 a.u. On the other hand, since the chemisorption energy of K on Al is substantially smaller than that of Na, the voltages producing atomic transfer are also much smaller (3–5 V).

Table I and Eq. (19) summarize well all the results for the surface induced by the applied voltages. Fig. 16 also shows the evolution of the adatom chemisorption energy just below the tip center as a function of the applied bias.

Fig. 16 is also important in order to analyze the non-linearity of the effects associated with the applied bias. As these curves show, the chemisorption energy does not change linearly with the voltage. In particular, the energy changes more slowly for positive biases (values for which the atom can be transferred from the tip to the sample). It is important to realize that this non-linearity is associated with the charge transfer induced on the system between the adatom and the metal. For positive voltages, the atom loses some electronic charge and becomes more ionic. Eventually, for high positive biases, the atom loses its electron charge completely and jumps to the tip in a bare ion state.

5. Discussion and concluding remarks

The results presented in this paper show how the electric field created by a voltage applied between a STM tip and a metal sample interacts with an alkali atom adsorbed on the metal. The method presented in this paper has allowed us to study that interaction for long lateral distances between the tip and the adsorbed atom. In particu-

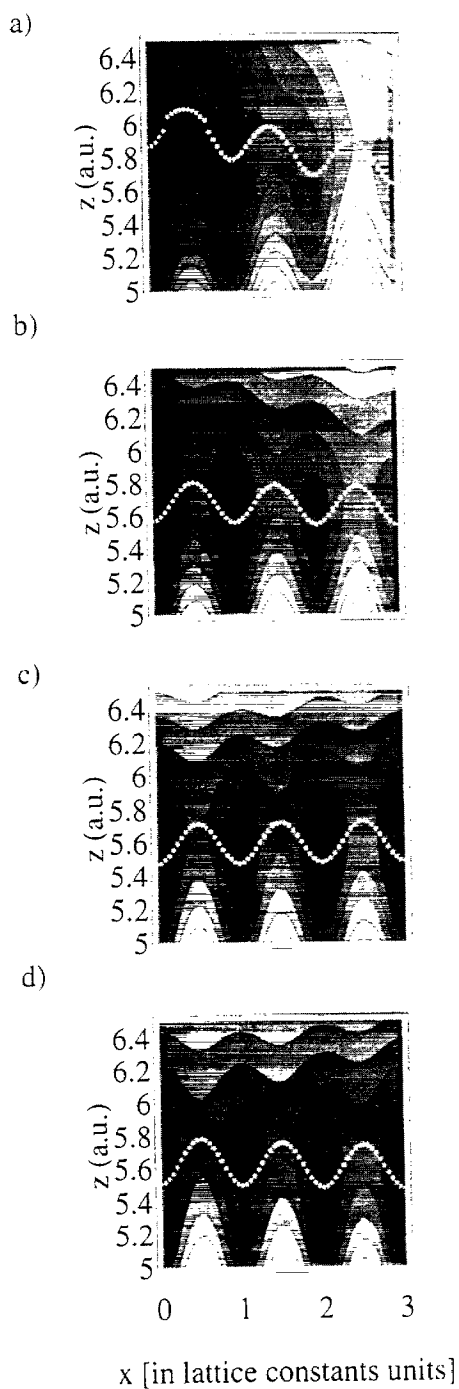


Fig. 7. As Fig. 4 for Na and $d=15$ a.u. (a) $V=6$ V, (b) $V=2$ V, (c) $V=-2$ V, (d) $V=-6$ V.

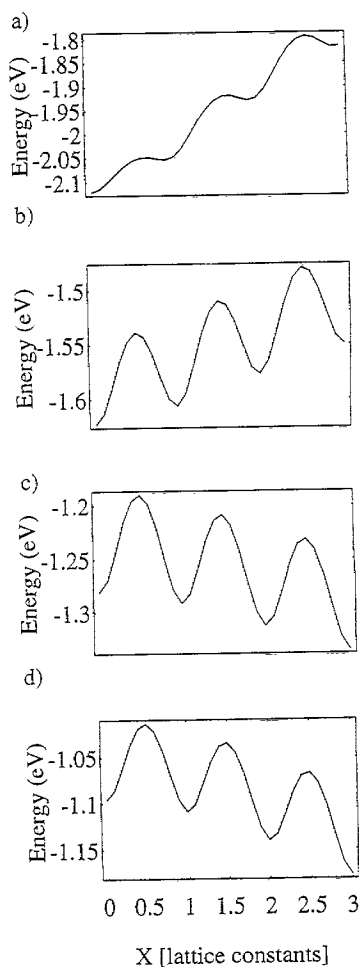


Fig. 8. As Fig. 5 for Na and $d=15$ a.u. (a) $V=6$ V, (b) $V=2$ V, (c) $V=-2$ V, (d) $V=-6$ V.

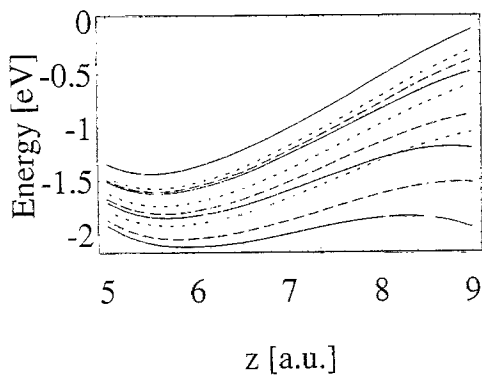


Fig. 9. As Fig. 6 for Na, $d=15$ a.u. and $V=0, 2, 4$ and 6 V.

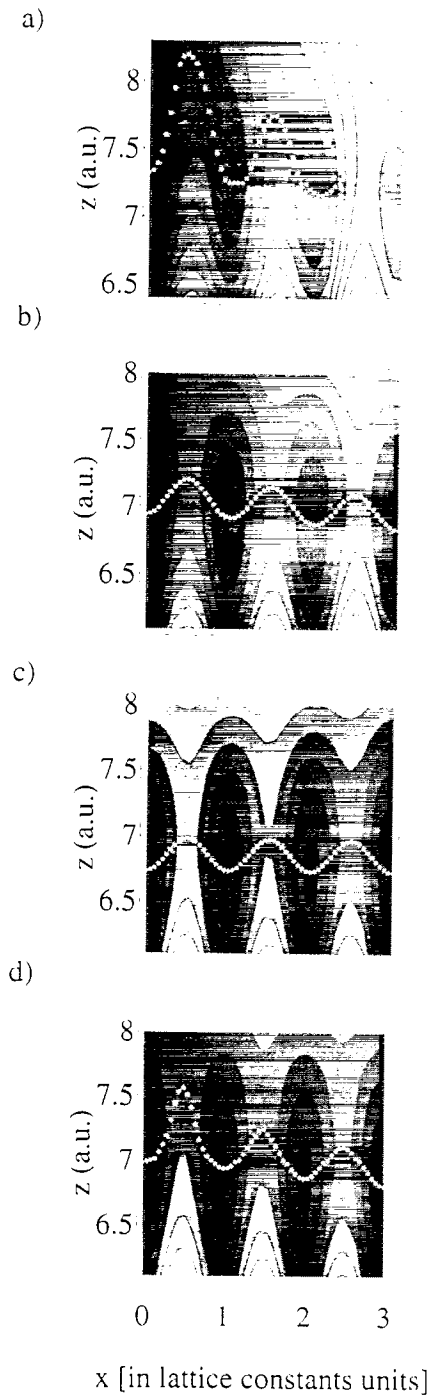


Fig. 10. As Fig. 4 for K and $d=19$ a.u. (a) $V=5$ V. (b) $V=2.5$ V. (c) $V=-2.5$ V. (d) $V=-5$ V.

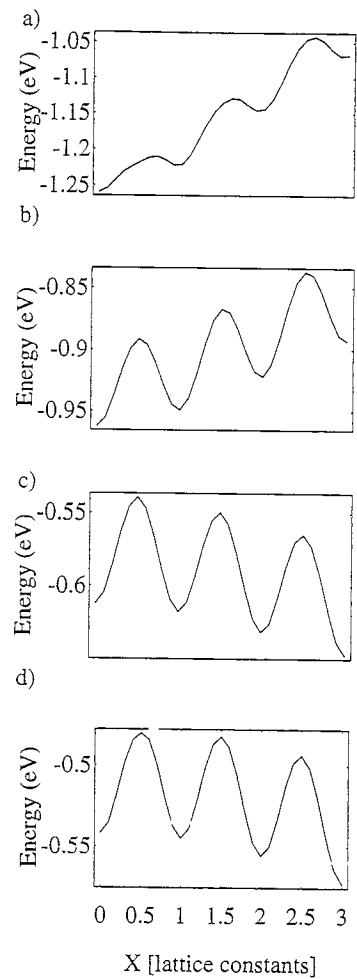


Fig. 11. As Fig. 5 for K and $d=19$ a.u. (a) $V=5$ V. (b) $V=2.5$ V. (c) $V=-2.5$ V. (d) $V=-5$ V.

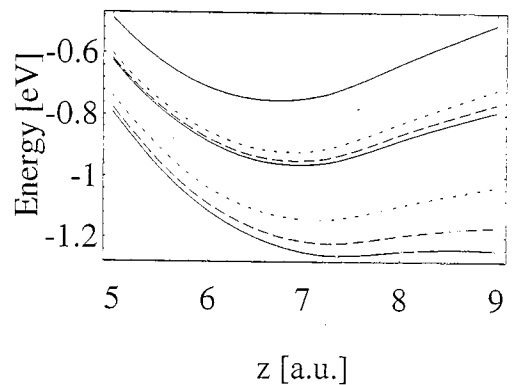


Fig. 12. As Fig. 6 for K , $d=19$ a.u. and $V=0, 2.5$ and 5 V.

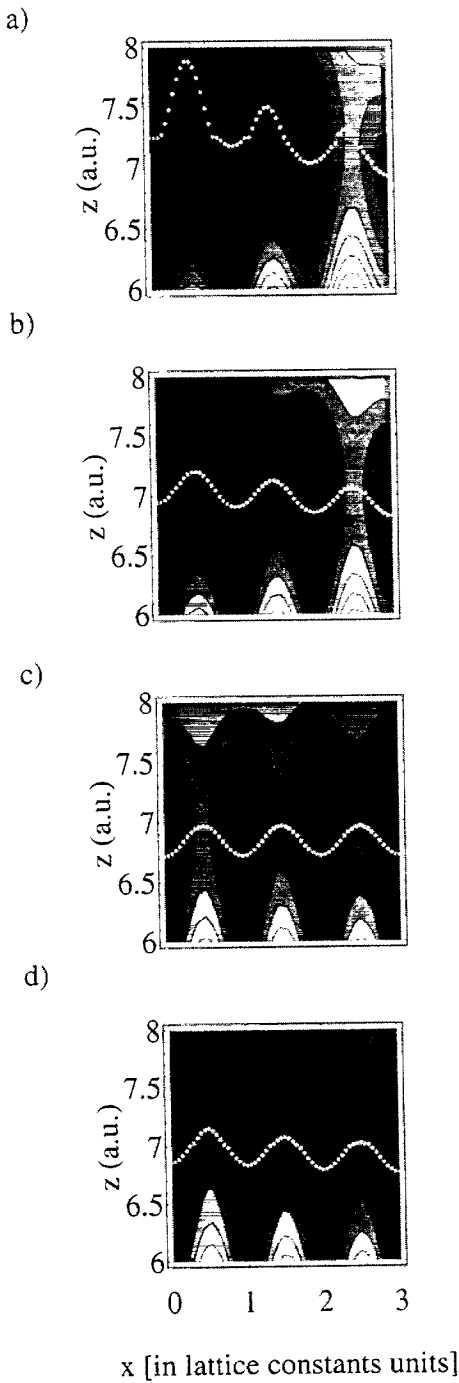


Fig. 13. As Fig. 4 for K and $d=17$ a.u. (a) $V=3.5$ V, (b) $V=2.0$ V, (c) $V=-2.0$ V, (d) $V=-3.5$ V.

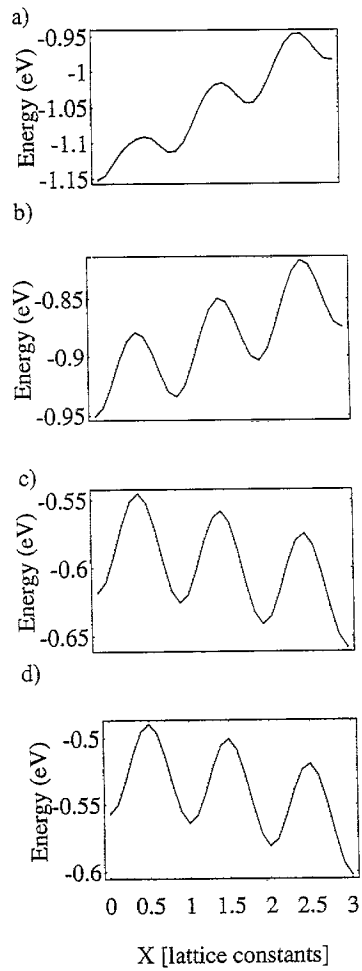


Fig. 14. As Fig. 5 for K and $d=17$ a.u. (a) $V=3.5$ V, (b) $V=2.0$ V, (c) $V=-2.0$ V, (d) $V=-3.5$ V.

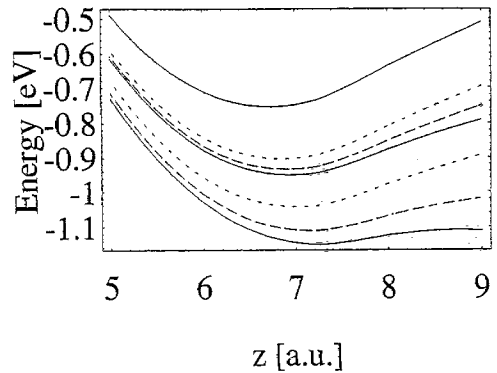


Fig. 15. As Fig. 6 for K. $d=17$ a.u. and $V=0, 2.0$ and 3.5 V.

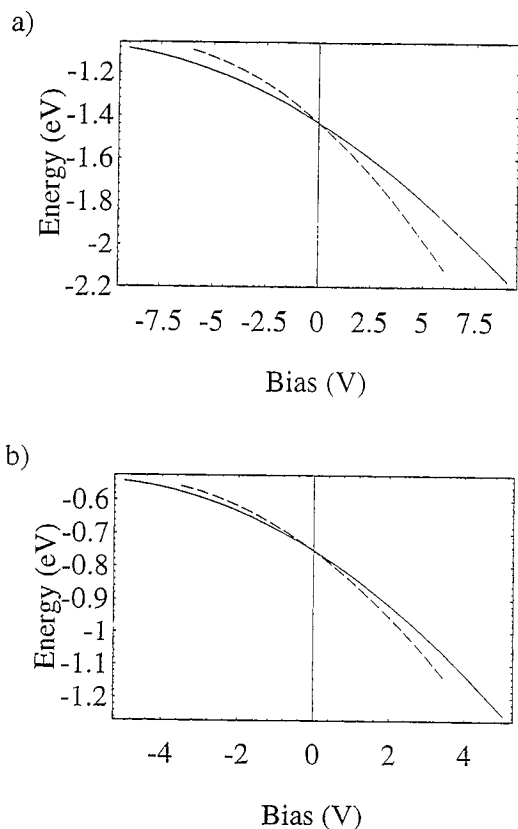


Fig. 16. Evolution of the chemisorption energy as a function of the applied voltage, for the alkali adsorbed at the hollow site under the tip ($x=0$). (a) Na. Solid line: tip located at 19 a.u. from the surface. Dotted line: tip located at 15 a.u. (b) K. Solid line: tip located at 19 a.u. from the surface. Dotted line: tip located at 17 a.u.

lar, this calculation gives information about the lateral forces the atom feels when adsorbed on the surface. Eq. (19) and Table 1 give a reasonable description of the potential well the tip creates just below it on the metal surface. Note that Eq. (19) has been chosen as the z -component of the electric field created at the metal interface by an external charge. This suggests that the chemisorption energy of the adsorbed atom is roughly proportional to the local value of E_z . It is interesting that for Na and a tip-sample distance of 19 a.u., the lateral barrier around the center of the well practically disappears for high positive voltages (around 9–11 V). For K and the same tip-sample distance, the lateral barrier is very small at 5–6 V. Similar

results are obtained for Na and $d=15$ a.u. if $V=6$ V; for K and $d=17$ a.u., the voltage of zero lateral barrier is only around 4 V.

In all these cases, we find that the lateral barrier around the center of the well has disappeared for voltages for which the atoms start to evaporate from the surface. The nominal evaporation fields for the cases studied in this paper are the following:

- (1) Na: $d=19$ a.u. $E=1.22 \text{ V \AA}^{-1}$,
- (2) Na: $d=15$ a.u. $E=0.91 \text{ V \AA}^{-1}$,
- (3) K: $d=19$ a.u. $E=0.52 \text{ V \AA}^{-1}$,
- (4) K: $d=17$ a.u. $E=0.41 \text{ V \AA}^{-1}$.

These values should be corrected by the effective field acting on the atom (see Figs. 3a and b). Taking into account the appropriate reduction factors, we find the following effective evaporation fields:

- (1) Na: $d=19$ a.u. $E^{\text{eff}}=0.58 \text{ V \AA}^{-1}$,
- (2) Na: $d=15$ a.u. $E^{\text{eff}}=0.55 \text{ V \AA}^{-1}$,
- (3) K: $d=19$ a.u. $E^{\text{eff}}=0.25 \text{ V \AA}^{-1}$,
- (4) K: $d=17$ a.u. $E^{\text{eff}}=0.22 \text{ V \AA}^{-1}$.

The effective evaporation fields for Na and K are practically independent of the tip-sample distance. This is the expected result if one can neglect the effect of the changes of the electric field in the direction parallel to the surface. The differences between Na and K are, however, important due to the very different chemisorption energies they have. The values given above should be compared with the evaporation fields calculated by other authors for a uniform electric field. Neugebauer and Scheffler [7] calculated 0.8 V \AA^{-1} for Na on the Al(111) surface, while Kahn and Ying [22] obtained 0.7 V \AA^{-1} for Na on jellium and 0.4 V \AA^{-1} for K. The experimental evaporation field [23] for Na and K on W(110), the only system for which we have found experimental information, is 0.6 and 0.36 V \AA^{-1} , respectively. These values are in reasonable agreement with our values, and show the same trends of our results. Probably, this mainly reflects the stronger bond of Na in both cases.

Our results should also be compared with those of Hirose and Tsukada [9], who analyzed the desorption of Na from a clean Na surface due to the field created by a Na tip located 14 a.u. from the metal surface. Their results suggest that a Na atom is transferred to the tip for a voltage close

to 5 V. The nominal evaporation field of this case is 0.68 V \AA^{-1} , and the effective evaporation field (using our own reduction factor as suggested by Fig. 3) is 0.30 V \AA^{-1} . This result should be compared with our previous values for the evaporation field. For Na on Al, we find an evaporation field which is twice as large as that given by Hirose and Tsukada. We think there are two explanations for this discrepancy. The first is associated with the different method used in the two calculations. In Hirose and Tsukada's approach, a 2×2 supercell is used and this model introduces spurious corrections due to the interaction between the ions in different supercells. In other words, in the 2×2 supercell, an atom jumping from the surface to the tip does it in a bare ion state and interacts simultaneously with equivalent ion states in different supercells. This interaction should correct the evaporation field calculated for a "single" atom, as done in our calculation. On the other hand, the Na–Na system analyzed by Hirose and Tsukada differs substantially from the Na–Al system analyzed in this paper. For Na chemisorbed on Na, Hirose and Tsukada calculated a chemisorption energy of 0.8 eV, a value which is more similar to the chemisorption energy we have obtained for K adsorbed on Al. This suggests that the evaporation field for the Na–Na interface should be more similar to the value calculated above for K on Al. It is difficult to judge, at this level, which effect is more important in explaining the difference between our results and those of Hirose and Tsukada. Probably, the difference in the chemisorption energy of the two systems is the dominant effect, modulated slightly by the different models used in the two calculations.

Returning to the atomic transfer process for fields close to the evaporation limit, it is worth noting that near this limit, the lateral and perpendicular barriers collapse almost simultaneously. Thus, we find that for the evaporation field the adsorbed atom can move almost freely, both on the metal sample (around the center of the well) and in the direction perpendicular to the surface from the center of the well to the tip. A good description of this behavior can be obtained from Figs. 4, 7, 10 and 13, where curves of constant chemisorption energy are drawn as a function of

the $x-z$ coordinates. Consider the cases for high positive bias, when the atom is close to the evaporation limit; in particular, look at Fig. 10, for K, $d=19$ a.u. and $V=5$ V. Fig. 10 shows how a very wide tube, of radius larger than a lattice constant, opens in the direction perpendicular to the surface: this is the region where the alkali atom moves in when being transferred from the sample to the tip. Notice also how the potential well for K evolves in the direction parallel to the surface (Fig. 11): after three lattice constants, that potential has gone up only by 0.2 eV. This is in agreement with the results shown in Table 1 for the potential well induced by the tip. Note how the width of the well increases for large positive voltages which develop a deeper and broader well.

Finally, we note that the results calculated in this paper have been obtained by assuming that the metal layers have no relaxation. Considering that the cohesive energy per atom for Al is much larger than the chemisorption energies of either Na or K, we can expect those relaxations to be unimportant, especially for K with a chemisorption energy of 0.8 eV. We cannot exclude, however, that some minor details, like changes in the potential barrier along the surface, could be affected by the metal relaxation layer [7].

In conclusion, we have presented an LCAO self-consistent calculation for analyzing the lateral forces acting on an alkali atom chemisorbed on a metal surface and located close to a tip. We have also calculated the evaporation field, and have presented a complete description of the surface potential controlling the atom's lateral diffusion and its sample–tip atomic transfer.

Acknowledgements

Support by Spanish CICYT (contract PB-92-0168c) is acknowledged. We also thank R. Pérez for helpful discussions.

References

- [1] E.W. Müller, Z. Phys. 131 (1951) 136.
- [2] G. Binnig, H. Rohrer, Ch. Gerber, E. Weibel, Phys. Rev. Lett. 49 (1982) 57.

- [3] D.M. Eigler, C.P. Lutz, W.E. Rudge, *Nature* 352 (1991) 600.
- [4] L.J. Whitman, J.A. Stroscio, R.A. Dragoscec, R.J. Celotta, in: Ph. Avouris (Ed.), *Atomic and Nanometer-Scale Modification of Materials*, Kluwer, Dordrecht, 1993.
- [5] H. Kuramochi, H. Uchida, M. Aono, *Phys. Rev. Lett.* 72 (1994) 932.
- [6] H.J. Kreuzer, L.C. Wang, N.D. Lang, *Phys. Rev. B* 45 (1992) 12050.
- [7] J. Neugebauer, M. Scheffler, *Surf. Sci.* 287 (1993) 572.
- [8] A. Buldum, S. Ciraci, *Phys. Rev. B* 54 (1996) 2175.
- [9] K. Hirose, M. Tsukada, *Phys. Rev. Lett.* 73 (1994) 150.
- [10] H.J. Kreuzer, *Surf. Sci.* 246 (1991) 336.
- [11] M. Sawamura, M. Tsukada, M. Aono, *Jpn. J. Appl. Phys.* 32 (1993) 3257.
- [12] S. Ciraci, E. Tekman, A. Baratoff, I.P. Batra, *Phys. Rev. B* 46 (1992) 10411.
- [13] J.R. Cerdá, P.L. de Andrés, F. Flores, R. Pérez, *Phys. Rev. B* 45 (1992) 8721.
- [14] F.J. García-Vidal, A. Martín-Rodero, F. Flores, J. Ortega, R. Pérez, *Phys. Rev. B* 44 (1991) 11412.
- [15] F.J. García-Vidal, J.-R. Merino, R. Pérez, R. Rincón, J. Ortega, F. Flores, *Phys. Rev. B* 50 (1994) 10537.
- [16] F. Guinea, C. Tejedor, F. Flores, E. Louis, *Phys. Rev. B* 28 (1983) 4397.
- [17] J. Ferrer, A. Martín-Rodero, F. Flores, *Phys. Rev. B* 38 (1988) 10113.
- [18] N. Mingo, L. Jurczyszyn, F.J. García-Vidal, R. Saiz-Pardo, P.L. de Andrés, F. Flores, S.Y. Wu, W. More, *Phys. Rev. B* 54 (1996) 2225.
- [19] J. Ortega, F. Flores, *Phys. Rev. Lett.* 63 (1989) 2500.
- [20] E. Clementi, C. Roetti, *At. Data Nucl. Data Tables* 14 (1974) 177.
- [21] D.A. Papaconstantopoulos, *Handbook of the Band Structure of Elemental Solids*, Plenum, New York, 1986.
- [22] L.M. Kahn, S.C. Ying, *Surf. Sci.* 59 (1976) 333.
- [23] C.J. Todd, T.N. Rhodin, *Surf. Sci.* 42 (1974) 109.